C: Surfaces, Interfaces, Porous Materials, and Catalysis

Reaction Pathway towards 7-Atom-Wide Armchair Graphene Nanoribbon Formation and Identification of Intermediate Species on Au(111)

Sebastian Thussing, Sebastian Flade, Kristjan Eimre, Carlo A. Pignedoli, Roman Fasel, and Peter Jakob

Just Accepted

Reaction Pathway towards 7-Atom-Wide Armchair Graphene Nanoribbon Formation and Identification of Intermediate Species on Au(111)

Sebastian Thussing,[†] Sebastian Flade,[†] Kristjan Eimre,[‡] Carlo A. Pignedoli,[‡] Roman Fasel,[‡,¶] and Peter Jakob[*,†]

[†]*Fachbereich Physik und Wissenschaftliches Zentrum für Materialwissenschaften der Philipps-Universität Marburg, Renthof 5, 35032 Marburg, Germany*

[‡]*Empa, Swiss Federal Laboratories for Materials, Science and Technology, 8600 Dübendorf, Switzerland*

[¶]*Department of Chemistry and Biochemistry, University of Bern, 3012 Bern, Switzerland*

E-mail: peter.jakob@physik.uni-marburg.de

Abstract

The prototypical surface reaction of 10,10'-dibromo-9,9'-bianthryl (DBBA) towards the 7-atom-wide armchair graphene nanoribbon (7-AGNR) on the Au(111) surface has been investigated by means of vibrational spectroscopy, thermal desorption spectroscopy and density functional theory. Specifically, a direct correlation between annealing temperature and the formation of various intermediate species is derived. By comparing IR spectra with results from DFT calculations an identification of reaction intermediates has been achieved, allowing for a precise mapping of individual reaction steps. Thereby, we identify a prior unknown partially dehalogenated and strongly tilted DBBA* mono-radical species (DBBA-1Br) after mild annealing (380 - 450 K). This

inclined adsorption geometry stabilizes the second Br atom, preventing full dehalogenation. According to our calculations dimerization of DBBA-1Br reverses this inclination and provides an efficient way to enable abstraction of the second Br atom and initiate polyanthracene chain formation by means of DBBA* addition. As a competitive process to dimerization a minor amount of the DBBA* mono-radicals recombine with previously released bromine atoms leading to associative DBBA desorption. In the course of thermal processing hydrogen release signals planarization of the twisted anthracene units of DBBA by means of cyclodehydrogenation and formation of the final 7-AGNR. Based on the results of this work an in-depth understanding of the on-surface synthesis of 7-AGNR on Au(111), starting with a DBBA molecular precursor, has been attained.

Introduction

Graphene nanoribbons (GNRs) are promising candidates for applications in nanoscale electronic devices due to their favorable electronic and optical properties,[1,2] as well as their excellent stability at ambient conditions.[3,4] The electronic properties of this material class can easily be modified by varying the GNR width,[1,5,6] the edge structure (armchair, zig-zag, chevron, chiral)[7,8] and the heteroatom dopant density.[9] However, the extremely sensitive relation between electronic and structural properties of graphene nanoribbons requires atomically precise fabrication techniques. This is most easily and efficiently achieved by means of on-surface synthesis,[10] even though numerous alternative techniques such as solution-based processing of GNRs,[11] unzipping carbon nanotubes[12] and lithographic approaches[2] have been examined. Thereby prototypes of high performance short channel field-effect transistors have already been successfully fabricated using this bottom-up approach.[13]

The most widely used method for on-surface synthesis of 1D-nanostructures is surface assisted Ullmann-coupling,[14] where halogenated precursor molecules are deposited on a metal surface. Upon annealing the halogen atoms detach from the precursor molecules (dehalogenation) and surface stabilized radicals are formed. These may either react among each other via direct C-C coupling or alternatively via organometallic intermediates to form elongated 1D-chains (polymerization). In a last step the polymerized species release hydrogen and neighboring carbon atoms react via C-C coupling to form a 1D strip of graphene (cyclodehydrogenation).

The chemical reactivities of the surface and the precursor molecules, especially the type of halogen atoms play a crucial role for the nanoribbon formation as competing reaction channels may lead to alternative final product species upon annealing. In the case of DBBA used as a precursor molecule (see scheme 1 for details), the influence of the chemical reactivity of the metal surface on the reaction pathway and the end product has been thoroughly investigated. For example, on copper surfaces full dehalogenation is found after depositing the precursor molecules at room temperature,[15–19] while the precursor molecules are only partially dehalogenated on silver surfaces;[16,20,21] on gold surfaces they remain intact as detachment of the halogen atoms requires notably higher annealing temperatures.[15,17,22,23] After dehalogenation has been accomplished the DBBA radicals link together to form 1D chains (polyanthracene) on Au(111),[10] whereas on Ag(111) and Cu(111) organometallic chains are formed by incorporating surface metal atoms.[21] On Ag(111) these organometallic chains eventually reorganize towards polyanthracene as well and, similar to Au(111), proceed towards the 7-AGNR; on Cu(111) the dehalogenated DBBA link together via C-C coupling resulting in the creation of chiral (3,1)-GNRs.[24] On the even more reactive Cu(110) substrate nanographene is produced instead of graphene nanoribbons, that is, polymerization is effectively suppressed.[18] One of the reasons is that cyclodehydrogenation of bianthryl monomers may proceed in parallel to polymerization of the precursor radicals for the more reactive substrates.[25] Hydrogen released during cyclodehydrogenation then may obstruct or terminate
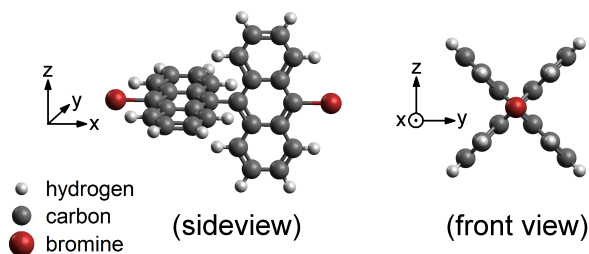
Scheme 1: Ball and stick model of DBBA including definition of the molecule's coordinate system. Note that DBBA vibrations with their dynamic dipole moments in the y- or z-direction are equivalent for the isolated molecule.

the polymerization process by saturating the carbon radical sites of the bianthryl monomers.

Interestingly, the temperature range for the dehalogenation process [26,27] (assumed to be the rate limiting step for polymerization) can be reduced by using precursor molecules with iodine instead of bromine. In this way notably longer GNR chains can be attained, as cyclodehydrogenation starts only after polymerization is completed. [28]

All in all the process of nanoribbon formation exhibits a complex reaction scheme that depends strongly on the chemical reactivity of the metal surface. In order to successfully design GNRs with specific properties it is thus essential to acquire in-depth information on the fundamental processes occurring in the course of the on-surface synthesis of nanostructures, the surface composition at any stage of the processing, as well as the prevalence of intermediate species.

The present work focuses on the reaction pathway of DBBA towards the 7-AGNR on the Au(111) surface and provides new insights in the highly relevant first step of dehalogenation of the DBBA precursor molecules. Thereby we take advantage of the characteristic vibrational signatures of the various molecular species, facilitating their identification and discrimination; thermal desorption spectroscopy (TDS) is used to examine various desorption channels and allow for a direct comparison with previous studies. In this way the reaction pathway along consecutive annealing steps has been explored. Specifically, a so far unknown transition state between the intact DBBA precursor and the polyanthracene chain, an inclined DBBA* mono-radical species has been found on Au(111). Recombination of these

to produce a DBBA dimer is suggested to facilitate abstraction of the second Br atom and trigger the polymerization process.

Methods

On-surface Synthesis and Characterization

All experiments were performed under ultra high vacuum (UHV) conditions with a base pressure of p = 5×10^{-11} mbar. The Au(111) single crystal (5N purity) is mounted to a liquid N_2 cooled cryostat. Linear heating rates can be applied by resistive heating and a computer-controlled power supply. Accurate temperature read-out was implemented using a K-type thermocouple (laser)welded to the edge of the Au single crystal. Prior to all measurements the Au surface was cleaned by Ar^+ sputtering (0.7 kV, I_{sample} = 1.3 μA, T_{sample} = 380 K, Δt = 30 min) and subsequent annealing to 780 K for 5 min. IRAS measurements were performed using a Bruker IFS 66v/s Fourier transform infrared spectrometer with evacuable optics (p < 10 mbar). The liquid N_2 cooled MCT (HgCdTe) detector allows for measurements in the spectral range 600 - 4000 cm^{-1}. All IR spectra were taken at a sample temperature of 80 K using an instrumental resolution of 2 cm^{-1} with typically 1000 scans coadded. We have employed the Origin8 software package to assemble individual IR spectra to a matrix that is used to create a 2D color-coded plot describing the thermal evolution of deposited DBBA on Au(111). IR spectra have been obtained after annealing to successively higher T (steps of 25K) and after recooling to 85K for data taking. We increased the matrix by a factor of 4 which corresponds to an interpolation of the data points between neighboring spectra; this creates a smoother transition between individual annealing steps but does not introduce new features. For thermal desorption measurements a quadrupole mass spectrometer (Pfeiffer, QMG 700, mass range 0 - 1024 u) was used to simultaneously collect several masses during linear heating. DBBA has been sublimated using a home-build evaporator with a typical deposition rate of 0.1 monolayer per minute (ML/min) at T_{DBBA} = 430 K. During deposition

the background pressure remained below 1×10^{-10} mbar. The (calibrated) molecular flux of the DBBA was monitored using the QMS during evaporation. A mass spectrum of the DBBA evaporant at a flux corresponding to 0.25 ML/min is provided in figure S1 of the Supporting Information.

Computational Procedures

The DFT calculations involving Au(111) slabs were performed with the CP2K code[29] utilizing the AiiDA platform.[30] The electronic states were expanded with a TZV2P Gaussian basis set[31] for C, H and Br species and a DZVP basis set for Au species. A cutoff of 600 Ry was used for the plane wave basis set. We used Norm Conserving Goedecker-Teter-Hutter[32] pseudopotentials and the PBE[33] exchange-correlation functional with the D3 dispersion corrections proposed by Grimme.[34] The surface/adsorbate systems were modeled within the repeated slab scheme, i.e. a simulation cell containing 4 atomic layers of Au along the [111] direction and a layer of hydrogen atoms to passivate one side of the slab in order to suppress one of the two Au(111) surface states. 40Å of vacuum were included in the simulation cell to decouple the system from its periodic replicas in the direction perpendicular to the surface. The Au(111) slabs used for the various DBBA conformations consisted of supercells of 41.27Å × 40.85Å corresponding to 224 surface units. To obtain the equilibrium geometries we kept the atomic positions of the bottom two layers of the slab fixed to the ideal bulk positions, all other atoms were relaxed until forces were lower than 0.0025 eV/Å. For the larger systems, the finite polyanthracene, 5^+-AGNR and 7-AGNR we used supercells of Au(111) slab with dimensions 106.13Å × 30.64Å corresponding to 432 surface units. Due to high computational cost and physisorbed nature of these systems, we left out the slab atoms from the DFT formalism and described the substrate-molecule interaction with an empirical potential.[35] For the geometry equilibration, all the slab atoms were fixed to positions corresponding to a clean (unreconstructed) Au(111) surface.

The vibrational analysis for all the adsorbate systems was performed with CP2K within

1
2
3
4
5
6
7
8
9
10
11
12
13
14
15
16
17
18
19
20
21
22
23
24
25
26
27
28
29
30
31
32
33
34
35
36
37
38
39
40
41
42
43
44
45
46
47
48
49
50
51
52
53
54
55
56
57
58
59
60

harmonic approximation by finite differences with a step of 0.001Å and a tolerance of 10^{-9} was used for the DFT self-consistent field iteration. Only the molecular atoms were displaced, keeping the slab fixed to obtain the normal modes of the adsorbate. The metal surface selection rule for the IR intensities was applied by taking only the dipole derivative contribution in the direction of the surface normal into account. To obtain the IR intensities the square of this component was considered. The spectra of polyanthracene, 5^{+}-AGNR and 7-AGNR were modified by filtering out modes defined by having more than 60% of their amplitude on the four anthracene units on either end of the chain/ribbon.

Results and Discussion

DBBA multilayers on Au(111)

In figure 1 infrared absorption spectra of increasing DBBA coverages (0.6 - 2.8 ML) deposited at 300 K on Au(111) are depicted in the frequency range of 640 - 1130 cm^{-1} (see also figure S2 of the Supporting Information). Moreover, vibrational frequencies for the DBBA gas phase molecule were calculated by density functional theory (DFT) with the PBE functional.[33] Derived line positions, including the respective direction of the corresponding dynamic dipole moments, either parallel to the Br - Br axis (x-direction, denoted as $\parallel$), or perpendicular to it (y/z direction, denoted as $\perp$), have been added at the bottom of the figure as vertical lines (the structure and coordinate system of the DBBA precursor molecule is defined in scheme 1).

After deposition at 300 K the DBBA molecules remain intact as dehalogenation[15,22] and polymerization[10] only set in at elevated surface temperatures (see below). The experimental line positions of the mono- and multilayer spectra match closely with those from the related anthracene molecule[36] and values from the DBBA calculations. A comparison between spectra of DBBA in direct contact with the Au(111) surface (top spectrum) with respect to multilayer DBBA yield clearly discernible, though weak line shifts, in accordance with
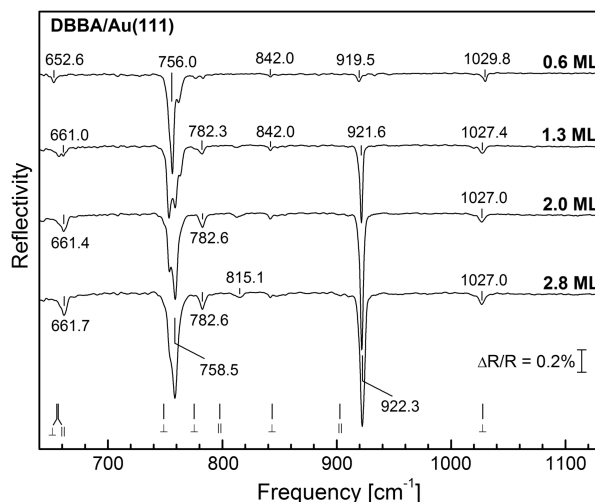
Figure 1: Infrared absorption spectra of DBBA deposited at 300 K on Au(111) for coverages of 0.6 - 2.8 ML, as indicated. Vertical lines at the bottom indicate the calculated vibrational line positions of the (free) DBBA molecule (strongest modes only); the directions of the respective dynamic dipole moments are given with respect to the Br - Br axis of DBBA, i.e. by adding a ∥ or ⊥ label. For better clarity of presentation the spectra are shifted vertically.

previous observations for similar systems. [37–39] Typically, for physisorbed or only weakly interacting adsorbates on a metal surface the frequency shifts between multilayer and the first layer are only marginal $(\Delta\nu < 10 \text{ cm}^{-1})$ [39–41] while for chemisorbed systems the frequency shifts are more severe $(\Delta\nu \approx 10 - 100 \text{ cm}^{-1})$. [38,39,42] Apparently, no strong interaction exists between the DBBA molecule and the Au(111) surface, in accordance with NEXAFS results [15] which excluded chemisorption for the present system.

The surface selection rule plays an important role in analyzing infrared spectra of molecules grown on metal surfaces since only vibrations with a dynamic dipole moment perpendicular to the metal surface can be excited. This is because components thereof aligned parallel to the metal surface are screened by their image dipoles. The most prominent mode of first-layer DBBA/Au(111) is located at 756.4 cm^{-1} and belongs to a vibration in y/z-direction. All x-type of modes display weak intensities, signaling an only slight inclination of the DBBA Br - Br axis with respect to the metal surface. By increasing the coverage beyond the first monolayer all vibrational modes gain intensity; however, those polarized in the x - direction to a much higher extent than those with their dynamic dipole moment in the y/z - direction.

We conclude that, starting with the second layer, the Br - Br axis becomes more strongly inclined.

DBBA monolayer on Au(111): Reaction pathway and intermediate species

The thermal evolution of DBBA on Au(111) is depicted in a 2D-plot with color-coded intensities (figure 2a). Thereby 0.8 ML DBBA has been deposited on Au(111) at 300 K and subsequently annealed to increasingly higher temperatures. From the evolution of vibrational mode intensities it is evident that the layer is subject to a series of transformations that include chemical reactions as well as conformational changes. Horizontal lines mark these transitions within the reaction pathway of DBBA $\rightarrow$ 7-AGNR and, in particular, help identifying intermediates.

In figure 2b we have selected three characteristic modes to monitor the abundances of the individual species and to describe the thermal evolution more quantitatively. Specifically, we have chosen the modes at about 756, 793 and 919 cm^{-1} as indicators for the presence of the twisted anthracene units, the 7-AGNR final product, and as a measure for the inclination of the (former) Br - Br axis, respectively.

After deposition at 300 K the IR spectra show a number of vibrational bands, the most prominent ones located at 756.4 cm^{-1} (μ_{dyn} in $\perp$ - direction) and at 919.4 cm^{-1} (μ_{dyn} in $\parallel$ - direction). From their intensity ratio and in accordance with figure 1 as well as figures 3 and 4 below, the presence of intact DBBA (also denoted as DBBA-2Br) is deduced, characterized by an only slightly inclined orientation of the Br - Br axis with respect to the Au(111) surface.

The primary activation of the DBBA species is initiated upon annealing to T > 380 K. This process is accompanied by a notable gain in intensity for vibrations with their dynamic dipole moments (μ_{dyn}) aligned along the $\parallel$ - direction (bands at 919, 1162, 1260 and 1302 cm^{-1}), while those with μ_{dyn} in the $\perp$ - direction (756, 842 and 1030 cm^{-1}) stay about constant or become weaker. Evidently, the Br - Br axis is now more strongly inclined
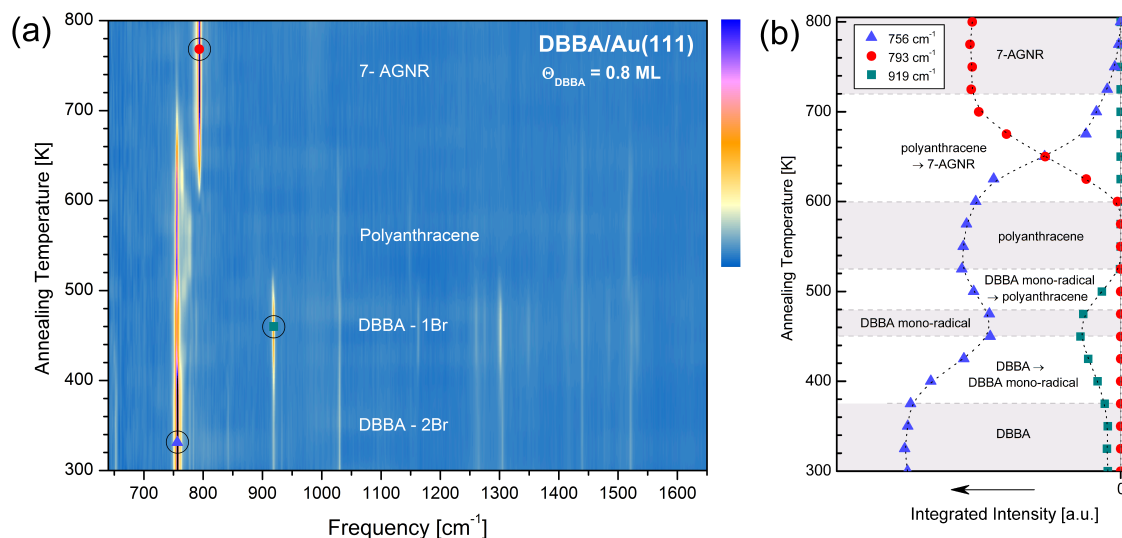
Figure 2: (a) 2D-plot of vibrational spectra with the color representing the absorption of the infrared light. The plot shows the thermal evolution of 0.8 ML DBBA deposited on Au(111) at 300 K and subsequent annealing to increasingly higher temperatures. All spectra have been recorded after recooling to 80 K. The coloring of the plot is adjusted to optimize the visibility of relevant features. (b) Thermal evolution of characteristic vibrational features of the layer in (a). The displayed signals refer to the integrated intensities of the bands at 756 (triangles), 793 (circles) and 919 cm^{-1} (squares) as indicated.

which is attributed to the abstraction of a Br atom and the formation of a chemical bond to a gold substrate atom. This conclusion is in agreement with XPS data that suggest detachment of bromine atoms at $T_{sample} = 375$ K;[15,22] specifically, two types of bromine species have been found in the temperature range of 375 - 475 K and attributed to Br atoms bound to either a carbon atom or the Au surface. The question whether both Br atoms detach concertedly or one after the other has not been addressed.

Based on our infrared-absorption spectroscopy (IRAS) data we suggest the following scenario: After detachment of the first bromine atom the unsaturated carbon atom of the anthracene subunit forms a new bond to the Au surface, and as a consequence the adsorption geometry switches to the aforementioned strongly inclined arrangement. Apart from the reported intensity variations the line shifts associated with this conformation change are surprisingly weak. We conclude that the overall integrity of the DBBA precursor molecule is largely retained. We will refer to this intermediate state as DBBA* mono-radical or

DBBA-1Br.

Quite naturally the inclined adsorption geometry of the DBBA* mono-radical species, along with the accordingly larger distance of the remaining Br atom to the Au surface, leads to an increased activation energy for detachment of this second bromine atom. In this way the inclined adsorption geometry will have a major impact on the overall dehalogenation process and successive reaction steps, e.g. the subsequent polymerization. It is likely that the formation of such a mono-radical species will likewise occur for other precursor molecules reacting towards 1D- or 2D-structures.

For a related system, bromobenzene on various noble metal surfaces (Au, Ag, Cu) a similar scenario has been suggested based on DFT calculation.[26] In their model a chemical bond between the unsaturated carbon atom of the benzene and a substrate atom is formed after detachment of the bromine atom. This new bond leads to a strong tilting of the molecular plane, i.e. the initially parallel orientation of the phenyl ring is lost. Thereby the tilt angle is found to increase with the strength of the molecule - metal interaction.

In the case of the partially dehalogenated DBBA on Cu(110) a strongly distorted molecular geometry has been suggested, with a strongly bent (former) Br-Br axis and with the dehalogenated anthracene subunit aligned more or less parallel to the metal surface.[18] For our DBBA/Au(111) system such a severely deformed molecular geometry is discarded as it would lead to notable overall frequency shifts, at variance to our observations. Instead, we suggest that the dehalogenated DBBA as a whole is inclined with respect to the Au(111) surface (thereby intensifying vibrations with a dynamic dipole moment in the $\parallel$ - direction), while the molecular structure is largely retained. We note that for the partially dehalogenated DBBA on Ag(111) a tilted adsorption geometry of the resulting mono-radical species has been suggested as well.[21]

Upon annealing to 520 K the IR spectra are subject to a dramatic change as virtually all modes with μ_{dyn} oriented along the $\parallel$ - direction vanish; $\perp$ - type of modes, on the other hand, are retained and even slightly gain in intensity. This is taken as unambiguous evidence

that the former Br - Br axis is now oriented parallel to the surface, most likely induced by detachment of the remaining bromine atoms. In accordance with literature data we conclude that at this stage of annealing dehalogenation is completed[15,22] and polymerization towards polyanthracene chains is in progress.[10]

Further annealing to 600 - 700 K leads to the gradual disappearance of the prominent anthracene mode at 756.4 cm^{-1} in favor of a new band emerging at 793.4 cm^{-1}. No other modes could be identified after heating to T > 720 K, suggesting that the mode at 793.4 cm^{-1} can be associated with the nanoribbon final product, and assigned to the out-of-plane bending mode of C-H bonds located at the rim of 7-AGNR.[43]

Interestingly, this transition is not abrupt but characterized by the coexistence of vibrational features associated with polyanthracene chains and 7-AGNR over an extended range of annealing temperatures. This observation is in accordance with findings in the literature[44] that cyclodehydrogenation of the polyanthracene chains towards 7-AGNR proceeds via a partially cyclized transitory species (5^{+}-AGNR) that will be discussed later.

DFT calculations of the 7-AGNR synthesis stages

In order to investigate the structural details of the 7-AGNR synthesis stages and their match with the experimental IR spectra, we performed density functional theory (DFT) calculations of the various stages along the reaction pathway of DBBA on Au(111) (figure 3); an overview of the manifold species and their adsorption geometries is depicted in figure S3 of the Supporting Information. We find that for both, the intact DBBA molecule and the DBBA* mono-radical, a flat as well as a tilted conformation on the Au(111) substrate exist, as depicted in figure S4 (Supporting Information). All the studied conformations of DBBA, the DBBA* mono-radical and the flat DBBA** di-radical show the prominent peak around 750 cm^{-1}; the characteristic experimentally observed band at around 900 cm^{-1} is, however, observed for the tilted configurations only. According to our calculations the flat DBBA is more stable than the tilted DBBA configuration by 0.21 eV; for the DBBA* mono-radical,
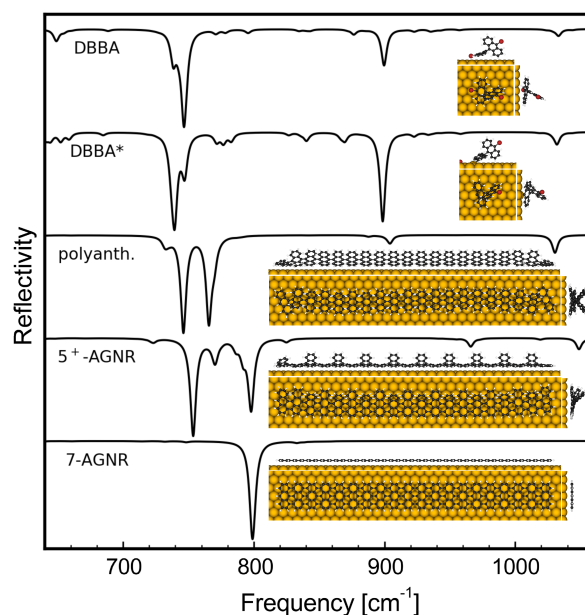
Figure 3: DFT-calculated IR spectra of the 7-AGNR synthesis stages on Au(111). The insets show the side and top views of the corresponding molecular species. The calculated spectra were obtained by broadening the discrete normal modes with a FWHM of 5 cm^{-1} and normalized to the highest peak. The spectra were reversed to more conveniently compare to experimental reflectivity results. Tilted conformations of intact DBBA and DBBA-1Br (DBBA*) were selected here since they show the mode aligned along the Br-Br axis around 900 cm^{-1} as is observed in the experiment.

the tilted conformation is practically energetically equal to the flat one (difference of 0.02 eV). This means that in the DBBA* mono-radical stage, considerably more molecules are in the tilted conformation compared to the fully brominated DBBA stage and therefore the vibrational modes ∥ to the Br-Br axis are considerably more intense, in accordance with experimental observations (figure 3).

The calculations for the polyanthracene, the 5^+-AGNR and 7-AGNR were performed on finite-length chains formed by the linking of 10 DBBA units. In the calculated IR spectra of these molecules, the vibrational modes at the chain ends are over-represented compared to the experiment where the formed chains are much longer. In order to obtain spectra comparable to the experiment, we filtered out those modes that had more than 60% of their amplitude on the four anthracene end units (for details see figure S5 of the Supporting Information). The results together with the tilted DBBA conformations are shown in figure 3.

In figure 4 selected IR spectra representative of the various intermediate species are depicted to aid comparison to calculated spectra in figure 3. We find that the experimentally observed infrared spectra show an excellent agreement with vibrational bands derived for according species on Au(111) using DFT calculations.

This comparison in particular allows an interpretation regarding the nature and the adsorption geometry of reaction species produced in the course of our annealing series. Thereby, the features at 919 and 1300 cm^{-1} with their dynamic dipole moments oriented along the direction of the (former) Br - Br axis play a central role to derive the detailed adsorption geometry (see also the calculated and experimentally observed IR spectra covering the frequency range 640 -1620 cm^{-1} in figures S4, S5, and S6 of the Supporting Information).

For DBBA-2Br, the DBBA-1Br mono-radical and to a lesser extent the polyanthracene species a fair number of calculated vibrational mode frequencies show only minute line shifts, especially for those associated with the DBBA core. This is actually not surprising as all three species contain the twisted anthracene units that, apparently, are still intact. The
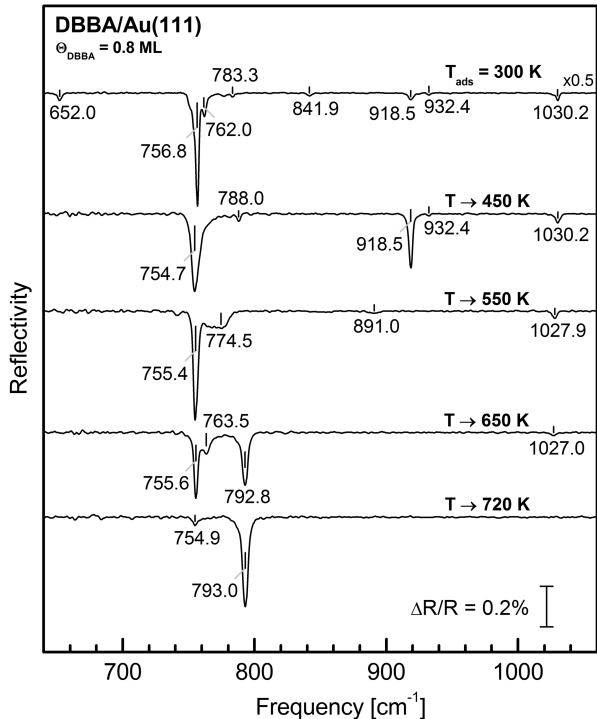
Figure 4: Vibrational signatures of intermediate species along the reaction of 0.8 ML DBBA towards the 7-AGNR on Au(111). The data were obtained after DBBA adsorption at 300 K (scaled by ×0.5) and after annealing to 450 K, 550 K, 650 K and 720 K (from top to bottom). All spectra have been taken after recooling to 80 K. For better clarity of presentation the curves are shifted vertically. According spectra covering the frequency range 640 - 1620 cm^{-1} are provided in the Supporting Information (figure S6).

influence of different binding partners at either end of the DBBA core (Br, Au, or C) on the vibrational spectra evidently is only minor. We do, however, observe a split-off feature of the 755 cm^{-1} band at around 775 cm^{-1} for the polymer chain (T $\approx$ 550 K). From their displacement patterns derived from the calculations they can be attributed to CH out-of-plane bending modes of the two top and the two bottom anthracene tips, respectively. The unusually broad appearance of the 775 cm^{-1} band might be associated with nearby surface Br atoms[45] causing extra line shifts and inhomogeneous broadening (ensemble average), or just caused by the close proximity to the gold substrate where the theoretical substrate-adsorbent interaction model is less applicable.

Upon annealing to T > 600 K a distinct alteration of the vibrational features in the 700 - 800 cm^{-1} frequency region is observed. This change is ascribed to the formation of the planar nanoribbon due to cyclodehydrogenation,[10] i.e. the coalescence of neighboring twisted anthracene subunits that comes with a release of hydrogen. According to figure 2 this process proceeds very gradually in the temperature range 600 - 720 K and, according to observations using scanning tunneling microscopy,[44] is accompanied by a transitory species connecting the polyanthracene chain and the 7-AGNR. This 5^{+}-AGNR species has undergone a complete transformation to the final nanoribbon product on one side of the polyanthracene chain while on the opposite side the twisted anthracene tips are preserved.

To examine the presence of the 5^{+}-AGNR intermediate species the respective IR spectrum obtained after annealing to 650 K has been included in figure 4. From the calculated spectra in figure 3 it is evident that the spectral region 700 - 800 cm^{-1} is not very specific regarding a discrimination of 5^{+}-AGNR from polyanthracene chains with admixtures of 7-AGNR. More distinct frequency shifts of vibrational bands are, however, expected in the region 900 - 1500 cm^{-1}. According to figures 2a and 4 no such shifts are observed and we must conclude that the amount of 5^{+}-AGNR species remains negligibly small at any stage of our processing (slow thermal annealing conditions). In fact, this finding is in accordance with aforementioned STM observations that, on the one hand have unambiguously identified

the 5^+-AGNR transitory configuration, while realizing that its abundance never exceeded the few percent level.[44] The evolution of IR spectra in figure 2a can thus be interpreted as a decreasing (increasing) amount of polyanthracene chains (7-AGNR final product), depending on the actual annealing temperature, while 5^+-AGNR constituting a minority species throughout.

Initial stages of DBBA polymerization on Au(111)

From figure 2b it is apparent that intensity variations of the modes at 756 cm^{-1} and 919 cm^{-1} band proceed in the same temperature range of 475 - 525 K and they are associated with the transformation of the DBBA to the polymer chains. The question arises which of the two processes (i) detachment of the second Br atom and (ii) the actual polymerization process comes first. In the following we discuss these two scenarios as model 1 and model 2, respectively.

Model 1 assumes that fully dehalogenated DBBA** di-radicals (DBBA-0Br) form first and they link together via the unsaturated carbon atoms of the anthracene subunits to form polyanthracene chains. Activation of DBBA-1Br, more precisely, abstraction of the second Br atom thereby sets in at elevated annealing temperatures only. This is because the strongly inclined geometry of the DBBA* mono-radical leads to an enlarged distance of the remaining bromine atom to the Au(111) surface, enhancing its thermal stability. The actual polymerization then occurs as a follow up process and most likely is associated with a lower activation barrier. This means that the rate limiting process in the formation of the polyanthracene chains would be the complete dehalogenation of DBBA, i.e. the detachment of the second Br atom from the DBBA-1Br species.

In an alternative model (model 2) polymerization is initiated by the dimerization of two DBBA-1Br units which leads to a considerably less inclined dimer species (planarization of the former Br-Br axis) and an accordingly closer distance of the remaining Br atoms to the Au(111) surface (see figure 5). As a consequence debromination of the dimer is facilitated,
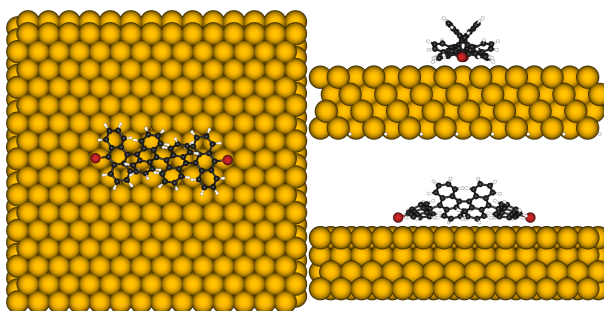
Figure 5: Adsorption geometry (top and side views) of a DBBA dimer species on Au(111) derived from DFT calculations.

enabling further attachment of DBBA-1Br species. The polymerization therefore proceeds in a two step manner: (i) debromination of the Br atom located at the end of the dimer or an existing polymer chain and (ii) attachment of another DBBA-1Br. In this way the polymer grows one-by-one until all DBBA-1Br are consumed (unless the polymer chain hits some boundary, or step edge, or else); of course, recombination of existing oligomers may occur as well at a later stage of the growth process. The fact that we do not observe the initial dimer species (see figure S4 of the Supporting Information) must not be interpreted as missing evidence; rather it is a natural consequence of the kinetics of the polymer growth, i.e. the instantaneous debromination once these DBBA dimer species are formed, in conjunction with a rapid attachment of nearby (abundant) DBBA-1Br. In model 2 the rate limiting process would be the formation of the $[\text{DBBA-1Br}]_2$ dimer species.

Model 2 is favored, though, as it naturally explains the formation of extended straight polymer chains and nanoribbon species; model 1, on the other hand, should lead to numerous rather short polymer units contrary to the observation in the literature. The problem in growing long chains according to model 1 is that fully debrominated DBBA is needed to grow the polymer chains and they form only gradually, while the species required for polyanthracene growth according to model 2, i.e. DBBA-1Br is amply available. We note that model 2 entirely avoids the formation of the fully dehalogenated DBBA-0Br species which plays an important role in the formation of nanographene platelets, e.g. on Ag(111) and Cu(110).[18,21]

Within the framework of polymer chain formation pioneered by P.J. Flory[46–48] the suggested reaction pathway may be described as chain initiation (rate limiting process of DBBA dimer formation), followed by a sequence of radical recombination (monomer addition) steps. We note that the recombination of two DBBA* radicals (chain initiation) as well as each of the radical recombination steps actually leads to a 'chain termination' of the produced species. A successful continuation of polymerization therefore relies on the surface to act as an omnipresent catalyst for monomer activation (as well as reactivation of existing chains after chain termination). According to our calculation this reactivation (abstraction of the remaining Br atom) is expedited by a structural rearrangement after monomer addition bringing the Br atoms much closer to the Au(111) surface and in this way easing its detachment (rapid reactivation after chain termination).

Thermal desorption spectroscopy

Thermal desorption traces of various DBBA fragments desorbing from the Au(111) surface are depicted in figure 6a. For that purpose, 2.8 ML DBBA have been deposited on Au(111) and subsequently annealed at a heating rate of 1 K/s. Besides intact DBBA (blue curve, mass 512 u) the desorption of H_2 (grey curve, mass 2 u) and HBr (red curve, mass 80 u) have been monitored. In agreement with Bronner et al.[45] the DBBA desorption signal can be subdivided in three sections, (i) multilayer desorption at 315 - 395 K, (ii) desorption from the 2nd DBBA layer at 395 - 450 K and (iii) desorption of first-layer DBBA at 450 - 530 K. Desorption of HBr and H_2 is restricted to the T - ranges 540 - 620 K and T > 620 K, respectively.

The desorption signal for first-layer DBBA is much smaller than for the second and higher layers, presumably due to a high probability for disintegration and formation of more strongly bound species. A similar set of desorption traces has been reported for CuPc/Ag(111) where on-surface dissociation likewise lead to negligible desorption signals of intact first-layer CuPc; instead desorption of CuPc fragments, namely $\frac{1}{4}$Pc was observed.[39] In order to clarify
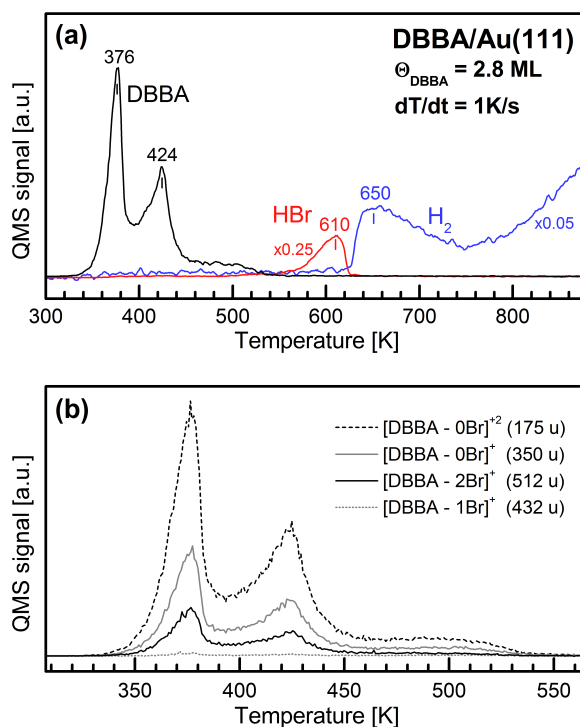
Figure 6: (a) Thermal desorption spectra (dT/dt = 1 K/s) of 2.8 ML DBBA/Au(111) deposited at T_{sample} = 300 K. The black, red and blue lines refer to desorption of DBBA (512 u), HBr (80 u) and H_2 (2 u), respectively. The signals of HBr and H_2 are scaled by a factor of 0.25 and 0.05, respectively. (b) Desorption traces of various fragments (as indicated in the figure) during multilayer desorption.

whether DBBA fragments desorb in appreciable amounts rather than reacting towards the 7-AGNR nanoribbon, the desorption signals of the most prominent DBBA fragments have been monitored (see figure 6b). The fragments were selected based on a mass scan of the DBBA flux during evaporation (see figure S1 of the Supporting Information for details): $[DBBA-1Br]^+$ (432 u), $[DBBA-0Br]^+$ (350 u) and $[DBBA-0Br]^{+2}$ (175 u). Evidently, all fragments show desorption traces identical to intact DBBA (512 u) for first-, second- and multilayers. Their presence is thus ascribed to fragmentation in the QMS ionization zone and we can safely exclude the independent desorption of DBBA fragments.

According to IRAS data (figures 2 and 4) the reaction of DBBA towards the DBBA* mono-radical is completed at 450 K. We note that the DBBA* species is available up to temperatures of about 500 K when polymerization of monomer units is induced by means of DBBA* attachment to DBBA dimer species and to polyanthracene chains. No intact DBBA should hence be present on the Au surface at temperatures of DBBA desorption from the monolayer. We conclude that the DBBA* mono-radicals react with coadsorbed atomic bromine that has accumulated on Au(111) after the first dehalogenation step. The observed weak DBBA desorption signal in the temperature range 450 - 530 K is thus entirely due to a recombinative desorption process. This actually implies that abstraction of the first Br atom represents a reversible process. We stress, however, that this first-layer recombinative desorption represents a minority reaction channel, that has negligible influence on the dominant reaction pathway, that comprises DBBA-dimer formation and subsequent polymerization.

We emphasize that under no circumstances could we ever observe desorption of DBBA mono- or di-radical species (as evidenced by mass 432 u or 350 u signals in the absence of mass 512 u; see figure 6b). This finding contradicts earlier reports by Bronner et al. who attributed their 176 u QMS signals to desorption of fully debrominated DBBA.[45] Specifically, the authors suggested that the Br atoms of the DBBA multilayer split off at the surface, resulting in desorption of a DBBA-0Br species. However, their conclusions were tainted by
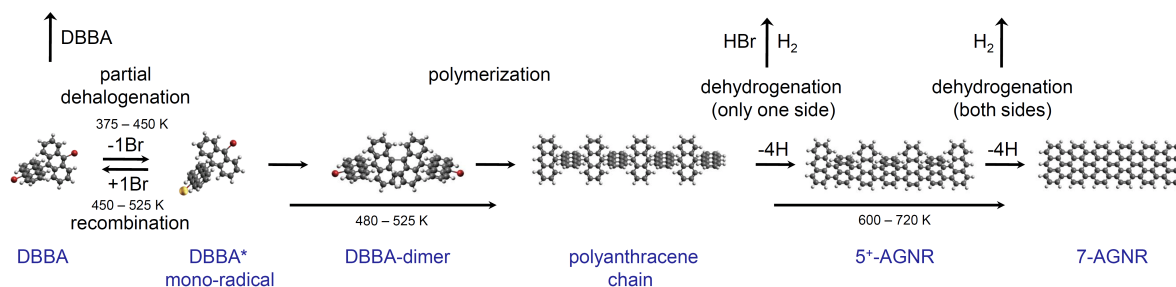
Figure 7: Schematic reaction pathway of DBBA towards 7-AGNR via the formation of DBBA mono-radicals and polyanthracene chains. Ball and stick model: carbon (grey), hydrogen (white), bromine (red), gold (golden).

the fact that mass 176 u had been used instead of the main 512 u mass to monitor DBBA desorption. Our TDS data in figure 6 (combined detection of mass 512 u, 350 u and 175 u desorption traces), on the other hand, clearly prove that multilayer DBBA desorbs intact and no dissociation occurs.

In the high temperature region (T > 550 K) HBr and H_2 represent the only desorbing species. In this temperature range hydrogen atoms are produced by means of cyclodehydrogenation of the polyanthracene chains. Interestingly, HBr desorption is completed before the evolution of molecular H_2 sets in at T > 630 K (see figure 6). According to DFT calculations by Bronner et al.[45] the activation barriers for HBr and H_2 desorption are very similar. The preferential desorption of HBr at T $\approx$ 600 K can therefore be associated with the difficulty of H atoms to find another H atom on the surface; the high abundance of Br atoms as a result of the complete dehalogenation of surface DBBA, on the other hand, ensures a high rate for HBr formation. Only after all Br is consumed released H atoms recombine and H_2 desorption sets in until the formation of the 7-AGNR is completed. The evolution of H_2 at T> 750 K is ascribed to the release of hydrogens at the rim of the 7-AGNR, in accordance with an intensity loss of the characteristic C-H bending mode at 793 cm^{-1}.

Conclusions

In our combined experimental and theoretical study we have used infrared absorption and thermal desorption spectroscopy to investigate the adsorption and thermal evolution of DBBA on Au(111). The main focus was to examine the reaction pathway of DBBA towards the 7-AGNR and identify reaction intermediates produced by thermal processing. Thereby structural parameters and vibrational signatures of the respective species have been derived from DFT calculations performed using the CP2K software. [29]

From the appearance and disappearance of characteristic vibrational bands the formation and decay of reaction intermediates has been deduced and transitory regimes assigned to specific temperature intervals. A summary of the reaction scheme describing the DBBA $\rightarrow$ 7-AGNR reaction pathway based on our findings and taking into account existing literature is depicted in figure 7.

We find that DBBA adsorbs intact on Au(111) with its Br - Br axis slightly inclined with respect to the metal surface. Thereby vibrational bands of first-layer and multilayer DBBA exhibit only minor frequency shifts with respect to free DBBA, in accordance with an only weak interaction between DBBA and Au(111). Annealing to 380 - 450 K leads to partial dehalogenation and the formation of a DBBA* mono-radical species with an adsorption geometry characterized by a strongly inclined (former) Br - Br axis. Upon further heating a small fraction of DBBA* mono-radicals recombines with previously detached bromine atoms to desorb as intact DBBA. The dominant reaction pathway of the DBBA* mono-radicals, however, involves DBBA-dimer formation as the thermodynamically limiting first reaction step towards polyanthracene formation, followed by continued attachment of DBBA*; eventually, extended polymer chains are formed, characterized by an orientation of the (former) Br - Br axis strictly parallel to the metal surface. This structural transformation quite naturally explains the absence of vibrations with a dynamic dipole moment in the $\parallel$ - directions in our IR - spectra. Annealing to 600 - 720 K induces cyclodehydrogenation of neighboring (twisted) anthracene subunits of the polymer chain towards the 7-AGNR final product,

with the 5^+-AGNR (one-sided dehydrogenated) species acting as an (undetected) transitory species that is present in minute amounts only.

Our results corroborate previous findings and complete the picture for the reaction of DBBA towards the 7-AGNR by identifying a novel inclined DBBA* mono-radical species and by assigning temperature intervals to the individual transitions between the various intermediate species. Our comparison of experimental and theoretical IR spectra in particular clarifies open questions regarding the adsorption geometry in the early stages of the processing not addressed so far. Thereby a model describing the initial stages of polyanthracene chain formation is suggested, comprising the dimerization of two DBBA* mono-radical species, followed by debromination and further attachment of DBBA*.

Associated Content

Supporting Information

Additional experimental and DFT-calculated IR spectra describing the coverage dependence and thermal evolution of deposited DBBA on Au(111); QMS mass spectra of the DBBA molecular beam; DFT-optimized geometries of various conformations of DBBA and reaction intermediates.

Acknowledgments

Author Information

Corresponding Author Email: peter.jakob@physik.uni-marburg.de

Tel.: +49-6421-2824328

ORCID Peter Jakob: 0000-0001-6478-309X

ORCID Sebastian Thussing: 0000-0002-8560-7682

ORCID Kristjan Eimre: 0000-0002-3444-3286

ORCID Carlo Antonio Pignedoli: 0000-0002-8273-6390

ORCID Roman Fasel: 0000-0002-1553-6487

Notes: The authors declare no competing financial interest.

References

(1) Son, Y.-W.; Cohen, M. L.; Louie, S. G. Energy Gaps in Graphene Nanoribbons. *Phys. Rev. Lett.* **2006**, *97*, 216803.

(2) Han, M. Y.; Özyilmaz, B.; Zhang, Y.; Kim, P. Energy Band-Gap Engineering of Graphene Nanoribbons. *Phys. Rev. Lett.* **2007**, *98*, 206805.

(3) Fairbrother, A.; Sanchez-Valencia, J.-R.; Lauber, B.; Shorubalko, I.; Ruffieux, P.; Hintermann, T.; Fasel, R. High Vacuum Synthesis and Ambient Stability of Bottom-Up Graphene Nanoribbons. *Nanoscale* **2017**, *9*, 2785–2792.

(4) Borin Barin, G. et al. Surface-Synthesized Graphene Nanoribbons for Room Temperature Switching Devices: Substrate Transfer and ex Situ Characterization. *ACS Appl. Nano Mater.* **2019**, *2*, 2184–2192.

(5) Barone, V.; Hod, O.; Scuseria, G. E. Electronic Structure and Stability of Semiconducting Graphene Nanoribbons. *Nano Lett.* **2006**, *6*, 2748–2754.

(6) Chen, Y.-C.; de Oteyza, D. G.; Pedramrazi, Z.; Chen, C.; Fischer, F. R.; Crommie, M. F. Tuning the Band Gap of Graphene Nanoribbons Synthesized from Molecular Precursors. *ACS Nano* **2013**, *7*, 6123–6128.

(7) Talirz, L.; Ruffieux, P.; Fasel, R. On-Surface Synthesis of Atomically Precise Graphene Nanoribbons. *Adv. Mater.* **2016**, *28*, 6222–6231.

(8) Nakada, K.; Fujita, M.; Dresselhaus, G.; Dresselhaus, M. S. Edge State in Graphene Ribbons: Nanometer Size Effect and Edge Shape Dependence. *Phys. Rev. B* **1996**, *54*, 17954–17961.

(9) Bronner, C.; Stremlau, S.; Gille, M.; Brausse, F.; Haase, A.; Hecht, S.; Tegeder, P. Aligning the Band Gap of Graphene Nanoribbons by Monomer Doping. *Angew. Chem. Int. Ed.* **2013**, *52*, 4422–4425.

(10) Cai, J.; Ruffieux, P.; Jaafar, R.; Bieri, M.; Braun, T.; Blankenburg, S.; Muoth, M.; Seitsonen, A. P.; Saleh, M.; Feng, X.; Müllen, K.; Fasel, R. Atomically Precise Bottom-Up Fabrication of Graphene Nanoribbons. *Nature* **2010**, *466*, 470–473.

(11) Li, X.; Wang, X.; Zhang, L.; Lee, S.; Dai, H. Chemically Derived, Ultrasmooth Graphene Nanoribbon Semiconductors. *Science* **2008**, *319*, 1229–1232.

(12) Kosynkin, D. V.; Higginbotham, A. L.; Sinitskii, A.; Lomeda, J. R.; Dimiev, A.; Price, B. K.; Tour, J. M. Longitudinal Unzipping of Carbon Nanotubes to form Graphene Nanoribbons. *Nature* **2009**, *458*, 872–876.

(13) Llinas, J. P. et al. Short-Channel Field-Effect Transistors with 9-Atom and 13-Atom Wide Graphene Nanoribbons. *Nat. Commun.* **2017**, *8*, 633.

(14) Lackinger, M. Surface-Assisted Ullmann Coupling. *Chem. Commun.* **2017**, *53*, 7872–7885.

(15) Simonov, K. A.; Vinogradov, N. A.; Vinogradov, A. S.; Generalov, A. V.; Zagrebina, E. M.; Martensson, N.; Cafolla, A. A.; Carpy, T.; Cunniffe, J. P.; Preobrajenski, A. B. Effect of Substrate Chemistry on the Bottom-Up Fabrication of Graphene Nanoribbons: Combined Core-Level Spectroscopy and STM Study. *J. Phys. Chem. C* **2014**, *118*, 12532–12540.

(16) Gutzler, R.; Cardenas, L.; Lipton-Duffin, J.; El Garah, M.; Dinca, L. E.; Szakacs, C. E.; Fu, C.; Gallagher, M.; Vondracek, M.; Rybachuk, M.; Perepichka, D. F.; Rosei, F. Ullmann-Type Coupling of Brominated Tetrathienoanthracene on Copper and Silver. *Nanoscale* **2014**, *6*, 2660–2668.

(17) Pham, T. A.; Song, F.; Nguyen, M.-T.; Li, Z.; Studener, F.; Stöhr, M. Comparing Ullmann Coupling on Noble Metal Surfaces: On-Surface Polymerization of 1,3,6,8-Tetrabromopyrene on Cu(111) and Au(111). *Chem. Eur. J.* **2016**, *22*, 5937–5944.

(18) Simonov, K. A.; Vinogradov, N. A.; Vinogradov, A. S.; Generalov, A. V.; Zagrebina, E. M.; Svirskiy, G. I.; Cafolla, A. A.; Carpy, T.; Cunniffe, J. P.; Taketsugu, T.; Lyalin, A.; Martensson, N.; Preobrajenski, A. B. From Graphene Nanoribbons on Cu(111) to Nanographene on Cu(110): Critical Role of Substrate Structure in the Bottom-Up Fabrication Strategy. *ACS Nano* **2015**, *9*, 8997–9011.

(19) Chen, M.; Xiao, J.; Steinrück, H.-P.; Wang, S.; Wang, W.; Lin, N.; Hieringer, W.; Gottfried, J. M. Combined Photoemission and Scanning Tunneling Microscopy Study of the Surface-Assisted Ullmann Coupling Reaction. *J. Phys. Chem. C* **2014**, *118*, 6820–6830.

(20) Eichhorn, J.; Strunskus, T.; Rastgoo-Lahrood, A.; Samanta, D.; Schmittel, M.; Lackinger, M. On-Surface Ullmann Polymerization via Intermediate Organometallic Networks on Ag(111). *Chem. Commun.* **2014**, *50*, 7680–7682.

(21) Simonov, K. A.; Generalov, A. V.; Vinogradov, A. S.; Svirskiy, G. I.; Cafolla, A. A.; McGuinness, C.; Taketsugu, T.; Lyalin, A.; Martensson, N.; Preobrajenski, A. B. Synthesis of Armchair Graphene Nanoribbons from the 10,10'-Dibromo-9,9'-Bianthracene Molecules on Ag(111): the Role of Organometallic Intermediates. *Sci. Rep.* **2018**, *8*, 3506.

(22) Batra, A.; Cvetko, D.; Kladnik, G.; Adak, O.; Cardoso, C.; Ferretti, A.; Prezzi, D.; Molinari, E.; Morgante, A.; Venkataraman, L. Probing the Mechanism for Graphene Nanoribbon Formation on Gold Surfaces through X-Ray Spectroscopy. *Chem. Sci.* **2014**, *5*, 4419–4423.

(23) Basagni, A.; Ferrighi, L.; Cattelan, M.; Nicolas, L.; Handrup, K.; Vaghi, L.; Papagni, A.; Sedona, F.; Valentin, C. D.; Agnoli, S.; Sambi, M. On-Surface Photo-Dissociation of C–Br bonds: Towards Room Temperature Ullmann Coupling. *Chem. Commun.* **2015**, *51*, 12593–12596.

(24) Sanchez-Sanchez, C.; Dienel, T.; Deniz, O.; Ruffieux, P.; Berger, R.; Feng, X.; Müllen, K.; Fasel, R. Purely Armchair or Partially Chiral: Noncontact Atomic Force Microscopy Characterization of Dibromo-Bianthryl-Based Graphene Nanoribbons Grown on Cu(111). *ACS Nano* **2016**, *10*, 8006–8011.

(25) Talirz, L.; Söde, H.; Cai, J.; Ruffieux, P.; Blankenburg, S.; Jafaar, R.; Berger, R.; Feng, X.; Müllen, K.; Passerone, D.; Fasel, R.; Pignedoli, C. A. Termini of Bottom-Up Fabricated Graphene Nanoribbons. *J. Am. Chem. Soc.* **2013**, *135*, 2060–2063.

(26) Björk, J.; Hanke, F.; Stafström, S. Mechanisms of Halogen-Based Covalent Self-Assembly on Metal Surfaces. *J. Am. Chem. Soc.* **2013**, *135*, 5768–5775.

(27) Bronner, C.; Marangoni, T.; Rizzo, D. J.; Durr, R. A.; Jorgensen, J. H.; Fischer, F. R.; Crommie, M. F. Iodine versus Bromine Functionalization for Bottom-Up Graphene Nanoribbon Growth: Role of Diffusion. *J. Phys. Chem. C* **2017**, *121*, 18490–18495.

(28) Di Giovannantonio, M.; Deniz, O.; Urgel, J. I.; Widmer, R.; Dienel, T.; Stolz, S.; Sanchez-Sanchez, C.; Muntwiler, M.; Dumslaff, T.; Berger, R.; Narita, A.; Feng, X.; Müllen, K.; Ruffieux, P.; Fasel, R. On-Surface Growth Dynamics of Graphene Nanoribbons: The Role of Halogen Functionalization. *ACS Nano* **2018**, *12*, 74–81.

(29) Hutter, J.; Iannuzzi, M.; Schiffmann, F.; VandeVondele, J. Cp2k: Atomistic Simulations of Condensed Matter Systems. *WIREs Comput. Mol. Sci.* **2014**, *4*, 15–25.

(30) Pizzi, G.; Cepellotti, A.; Sabatini, R.; Marzari, N.; Kozinsky, B. AiiDA: Automated Interactive Infrastructure and Database for Computational Science. *Comp. Mater. Sci.* **2016**, *111*, 218–230.

(31) VandeVondele, J.; Hutter, J. Gaussian Basis Sets for Accurate Calculations on Molecular Systems in Gas and Condensed Phases. *J. Chem. Phys.* **2007**, *127*, 114105.

(32) Goedecker, S.; Teter, M.; Hutter, J. Separable Dual-Space Gaussian Pseudopotentials. *Phys. Rev. B* **1996**, *54*, 1703–1710.

(33) Perdew, J. P.; Burke, K.; Ernzerhof, M. Generalized Gradient Approximation Made Simple. *Phys. Rev. Lett.* **1996**, *77*, 3865–3868.

(34) Grimme, S.; Antony, J.; Ehrlich, S.; Krieg, H. A Consistent and Accurate Ab Initio Parametrization of Density Functional Dispersion Correction (DFT-D) for the 94 Elements H-Pu. *J. Chem. Phys.* **2010**, *132*, 154104.

(35) Pignedoli, C. A.; Laino, T.; Treier, M.; Fasel, R.; Passerone, D. A Simple Approach for Describing Metal-Supported Cyclohexaphenylene Dehydrogenation - Hybrid Classical/DFT Metadynamics Simulations. *Eur. Phys. J. B* **2010**, *75*, 65–70.

(36) Hudgins, D. M.; Sandford, S. A. Infrared Spectroscopy of Matrix Isolated Polycyclic Aromatic Hydrocarbons. 1. PAHs Containing Two to Four Rings. *J. Phys. Chem. A* **1998**, *102*, 329–343.

(37) Thussing, S.; Jakob, P. Thermal Stability and Interlayer Exchange Processes in Heterolayers of CuPc and PTCDA on Ag(111). *J. Phys. Chem. C* **2017**, *121*, 13680–13691.

(38) Zaitsev, N. L.; Jakob, P.; Tonner, R. Structure and Vibrational Properties of the PTCDA/Ag(111) Interface: Bilayer versus Monolayer. *J. Phys.: Condens. Matter* **2018**, *30*, 354001.

(39) Thussing, S.; Jakob, P. Structural and Vibrational Properties of CuPc/Ag(111) Ultrathin Films. *J. Phys. Chem. C* **2016**, *120*, 9904–9913.

(40) Auerhammer, J. M.; Knupfer, M.; Peisert, H.; Fink, J. The Copper Phthalocyanine/Au(100) Interface Studied Using High Resolution Electron Energy-Loss Spectroscopy. *Surf. Sci.* **2002**, *506*, 333 – 338.

(41) Eremtchenko, M.; Bauer, D.; Schaefer, J. A.; Tautz, F. S. Polycyclic Aromates on Close-Packed Metal Surfaces: Functionalization, Molecular Chemisorption and Organic Epitaxy. *New J. Phys.* **2004**, *6*, 4.

(42) Fernández, L.; Thussing, S.; Mänz, A.; Sundermeyer, J.; Witte, G.; Jakob, P. The Discrete Nature of Inhomogeneity: The Initial Stages and Local Configurations of TiOPc During Bilayer Growth on Ag(111). *Phys. Chem. Chem. Phys.* **2017**, *19*, 2495–2502.

(43) Bronner, C.; Leyssner, F.; Stremlau, S.; Utecht, M.; Saalfrank, P.; Klamroth, T.; Tegeder, P. Electronic Structure of a Subnanometer Wide Bottom-Up Fabricated Graphene Nanoribbon: End States, Band Gap, and Dispersion. *Phys. Rev. B* **2012**, *86*, 085444.

(44) Blankenburg, S.; Cai, J.; Ruffieux, P.; Jaafar, R.; Passerone, D.; Feng, X.; Müllen, K.; Fasel, R.; Pignedoli, C. A. Intraribbon Heterojunction Formation in Ultranarrow Graphene Nanoribbons. *ACS Nano* **2012**, *6*, 2020–2025.

(45) Bronner, C.; Björk, J.; Tegeder, P. Tracking and Removing Br during the On-Surface Synthesis of a Graphene Nanoribbon. *J. Phys. Chem. C* **2015**, *119*, 486–493.

(46) Flory, P. J. Molecular Size Distribution in Linear Condensation Polymers. *J. Am. Chem. Soc.* **1936**, *58*, 1877–1885.

(47) Flory, P. J. The Mechanism of Vinyl Polymerizations. *J. Am. Chem. Soc.* **1937**, *59*, 241–253.

(48) Flory, P. J. *Principles of Polymer Chemistry*; Cornell University Press: Ithaca, New York, 1953.

TOC graphic